Hindawi
Mathematical Problems in Engineering
Volume 2017, Article ID 1805091, 14 pages
https://doi.org/10.1155/2017/1805091

Research Article

Applications of an Improved Time-Frequency Filtering Algorithm to Signal Reconstruction

Junbo Long,[1] Haibin Wang,[2] Daifeng Zha,[3] Hongshe Fan,[1] Zefeng Lao,[1] and Huajie Wu[1]

[1]*College of Electronic and Engineering, Jiujiang University, Jiujiang, China*
[2]*College of Information Science and Engineering Technology, Jiujiang University, Jiujiang, China*
[3]*College of Science, Jiujiang University, Jiujiang, China*

Correspondence should be addressed to Junbo Long; 18488870@qq.com

Received 11 January 2017; Revised 28 March 2017; Accepted 6 April 2017; Published 8 May 2017

Academic Editor: Denis Benasciutti

The short time Fourier transform time-frequency representation (STFT-TFR) method degenerates, and the corresponding short time Fourier transform time-frequency filtering (STFT-TFF) method fails under α stable distribution noise environment. A fractional low order short time Fourier transform (FLOSTFT) which takes advantage of fractional p order moment is proposed for α stable distribution noise environment, and the corresponding FLOSTFT time-frequency representation (FLOSTFT-TFR) algorithm is presented in this paper. We study vector formulation of the FLOSTFT and inverse FLOSTFT (IFLOSTFT) methods and propose a FLOSTFT time-frequency filtering (FLOSTFT-TFF) method which takes advantage of time-frequency localized spectra of the signal in time-frequency domain. The simulation results show that, employing the FLOSTFT-TFR method and the FLOSTFT-TFF method with an adaptive weight function, time-frequency distribution of the signals can be better gotten and time-frequency localized region of the signal can be effectively extracted from α stable distribution noise, and also the original signal can be restored employing the IFLOSTFT method. Their performances are better than the STFT-TFR and STFT-TFF methods, and MSEs are smaller in different α and GSNR cases. Finally, we apply the FLOSTFT-TFR and FLOSTFT-TFF methods to extract fault features of the bearing outer race fault signal and restore the original fault signal from α stable distribution noise; the experimental results illustrate their performances.

1. Introduction

The time-frequency analysis method is an effective tool for nonstationary signal processing, which has been broadly used in communication, acoustics, mechanical signal processing, medical signal processing, and others [1–5]. Short time Fourier transform time-frequency representation (STFT-TFR) has a rich structure with dependencies along both the time and frequency axes, which is widely applied in speech [6, 7], communication [8, 9], and others [10, 11]. A speech enhancement algorithm employing the STFT-TFR method is presented in [6], which takes advantage of the time and frequency dependencies of speech signals. An improved method which can reconstruct the spectral phase of the speech signal is proposed in [7]; the method only depends on the fundamental frequency and the noisy observation from the STFT domain. An interference excision algorithm is proposed for direct-sequence spread spectrum communication systems [8, 9], which analyze the interference in STFT time-frequency domain and detect and estimate the high-power jamming signal employing inverse STFT (ISTFT). Abdullah et al. apply the STFT-TFR method to analyze the switches faults of three-phase voltage source inverter [10]. Zhang et al. propose a time-frequency MUSIC algorithm employing the STFT-TFR method in [11], which is applied to estimate the DOAs of the closely spaced sources.

The time-frequency filtering technology which takes advantage of time-frequency localized spectra of the data provides an adaptive filtering method for the nonstationary signals. The time-frequency filtering method applies an adaptive weighting function to separate out the signals from the noise. The higher weighting parts localize the regions which are

expected to be the signal components, and the lower weighting parts attenuate the noise in the time-frequency domain. The inverse transform of time-frequency representation is used to reconstruct the original signals. Recently, an adaptive time-frequency filtering method employing the Stockwell transform time-frequency representation (ST-TFR) method and its inverse transform are used to analyze the earthquake data [12, 13]; WANG et al. propose a new time-frequency filtering method employing normalized window S transform and TT transform in [14], which is applied to attenuate high frequency noise and random noise for the radar echo signal. An adaptive filtering method employing generalized S transform is presented in [15], which is constructed by a new adaptive time-frequency filtering factor, and the method is applied to restore the LFM signals from the noise. A generalized S transform is presented in [16], which is used to extract the special signal components and filter out the noise. CHI et al. propose an adaptive time-frequency filtering method based on the STFT-TFR method and apply it to filter out the noise in FM signal; the results demonstrate that the time-frequency filtering method is effective for FM signal filtering [17]. A FM interference suppression method employing the STFT-TFR and time-frequency filtering is presented in [18], which is applied to suppress the interference in the FM signals and improve the correlation output. Yang proposed an inverse STFT method and studied its vector formulation in [19].

The Gaussian noise is assumed in the above time-frequency representation methods and time-frequency filtering methods, and second-order statistics is applied to analyze the signals. In general cases, Gaussian hypothesis is reasonable, and the above methods are effective. However, in some actual signals such as the mechanical bearing fault signals, electroencephalogram, and radar signal, the noise has obvious pulsing characteristics, and the noise is non-Gaussian and nonstationary α stable distribution [20–26]. When $\alpha = 2$, the noise belongs to Gaussian distribution, and when $0 < \alpha < 2$, it is low order α stable distribution. In low-order α stable distribution environment, the mentioned methods in [12–19] are based on second-order statistics, and their performance will degenerate when Gaussian model is employed to analyze the non-Gaussian signals. Recently, α stable distribution model is used for the bearing fault signals diagnosis in [27–30]. Fractional lower order statistic is applied to extract the evoked potential in [31, 32]. In α stable distribution environment, the STFT-TFR method in the literature [8–11] degrades and even fails. Therefore, the corresponding time-frequency filtering method employing the STFT-TFF method in [17–19] degenerates. Hence, we propose fractional lower order short time Fourier transform and its inverse transform and propose a fractional lower order short time Fourier transform time-frequency representation (FLOSTFT-TFR) method for α stable distribution noise environment. Based on the proposed FLOSTFT-TFR and IFLOST methods, we present a novel fractional lower order short time Fourier transform time-frequency filtering (FLOSTFT-TFF) algorithm which takes advantage of time-frequency localized spectra of the signal in time-frequency domain in this paper. The simulations show that the FLOSTFT-TFR method can better demonstrate time-frequency distribution of the signals, the FLOSTFT-TFF method can effectively restore the original signal under α stable distribution noise environment, their performances are better than the STFT-TFR and STFT-TFF methods, and their MSEs are smaller under different α and GSNR. We apply the FLOSTFT-TFR and FLOSTFT-TFF methods to extract fault features of the bearing outer race fault signal and restore the original fault signal from α stable distribution noise, which illustrate their performances. Hence, the FLOSTFT-TFR method provides an approach for the special time-frequency analysis cases. IFLOSTFT is inverse transform of FLOSTFT, which provides a computational efficient way to restore the original signal from its time-frequency distribution when the undesired parts are removed.

In this paper, an improved time-frequency representation method employing fractional low order moment is proposed for α stable distribution noise environment, and a novel time-frequency filtering method is presented. The paper is structured in the following manner. α stable distribution is introduced in Section 2. In Section 3 we demonstrate a fractional low order short time Fourier transform and its inverse transform, the vector formulation of FLOSTFT and IFLOSTFT are derived, and the improved time-frequency representation is studied. The improved fractional lower order time-frequency filtering method is demonstrated in Section 4. The simulations are performed to demonstrate justifiability of the proposed time-frequency representation and time-frequency filtering methods based on FLOSTFT and IFLOSTFT, and the simulations of the outer race fault signals diagnosis are demonstrated in Section 5. Finally, the discussions and conclusions are given in Sections 6 and 7, respectively.

2. α Stable Distribution

The characteristic function of α stable distribution can be defined as [20, 21]

$$\varphi(t) = \exp\left\{j\mu t - \gamma |t|^{\alpha} \left[1 + j\beta \operatorname{sign}(t)\, \omega(\tau, \alpha)\right]\right\} \quad (1a)$$

$$\omega(\tau, \alpha) = \begin{cases} \tan\left(\dfrac{\alpha\pi}{2}\right) & \text{if } \alpha \neq 1 \\ \left(\dfrac{2}{\pi}\right) \log|\tau| & \text{if } \alpha = 1, \end{cases}$$

$$\operatorname{sign}(t) = \begin{cases} 1 & t > 0 \\ 0 & t = 0 \\ -1 & t < 0, \end{cases} \quad (1b)$$

where $\alpha \in (0, 2]$ is the characteristic index; it determines the pulse degree of α stable distribution. If $\alpha = 2$, X is Gaussian distribution; if $\alpha \in (0, 2)$, X is non-Gaussian fractional lower order distribution. Parameter γ is the dispersion coefficient, parameter μ is the location parameter, and parameter β is the symmetry coefficient. If the parameter $\beta = 0$, X is called symmetric α stable distribution (SαS), its characteristic

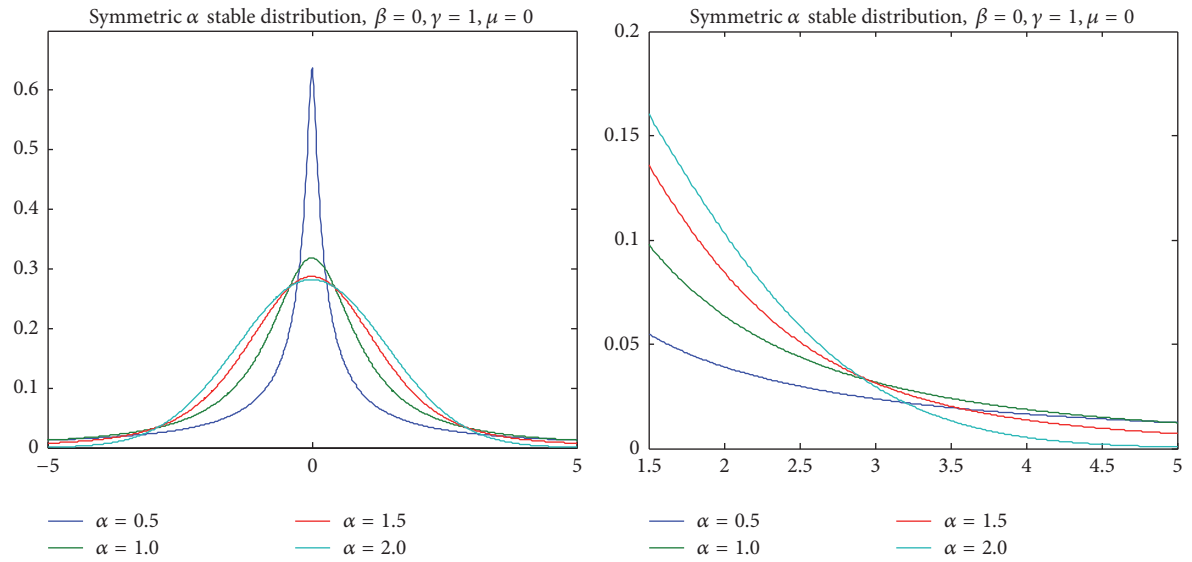

Figure 1: PDFs of SαS stable distribution in different α.

function can be expressed as (2), and when $\alpha = 2$, which is the same as the characteristic function of Gaussian distribution,

$$\phi(t) = \exp\left\{j\mu t - \gamma |t|^{\alpha}\right\}. \tag{2}$$

Probability density functions (PDFs) of SαS are given under $\alpha = 0.5$, $\alpha = 1.0$, $\alpha = 1.5$, and $\alpha = 2.0$ in Figure 1.

3. FLOSTFT and Its Inverse Transform

3.1. FLOSTFT. Fractional p order moment of the signal $x(t)$ is defined as

$$\widetilde{x}(t) = x^{\langle p\rangle}(t), \tag{3}$$

where $\langle p\rangle$ is p order moment operation of $x(t)$. When $x(t)$ is a real signal, $x^{\langle p\rangle}(t) = |x(t)|^{p-1} \cdot \operatorname{sign}[x(t)]$, and when $x(t)$ is a complex signal, $x^{\langle p\rangle}(t) = |x(t)|^{p-1} \cdot x^{*}(t)$. p is a real parameter, and $1 \le p \le 2$ [21, 22], $*$ demonstrate conjugate. Both sides of (3) are multiplied by a real window function $h(t)$ centered at time $\tau = t$, and localized spectrum of $\widetilde{x}(t)$ at $\tau = t$ is obtained, as shown in

$$\widetilde{S}_h(t,\tau) = \widetilde{x}(t)\, h(\tau - t) = x^{\langle p\rangle}(t)\, h(\tau - t). \tag{4}$$

After (4) has taken Fourier transform to time τ, we obtain

$$\begin{aligned} \mathrm{FLOSTFT}_x(t,f) &= \underset{\tau\to f}{F}\left\{\widetilde{x}(t)\, h(\tau - t)\right\} \\ &= \underset{\tau\to f}{F}\left\{x^{\langle p\rangle}(t)\, h(\tau - t)\right\} \end{aligned} \tag{5}$$

$$\mathrm{FLOSTFT}_x(t,f) = \int_{-\infty}^{+\infty} x^{\langle p\rangle}(t)\, h(\tau - t)\, e^{-j2\pi f\tau} d\tau. \tag{6}$$

Equation (6) is called fractional low order short time Fourier transform (FLOSTFT); the corresponding discrete FLOSTFT can be written as

$$\mathrm{FLOSTFT}_x(n,\omega) = \sum_{m} x^{\langle p\rangle}(m)\, h(m - n)\, e^{-j\omega n}. \tag{7}$$

3.2. Computation of FLOSTFT. The discrete form of $x(t)$ can be expressed as $x(n)$, $n = 0, 1, \ldots, N-1$; then its discrete fractional p order moment in (3) is written as

$$\begin{aligned} &\widetilde{x}(n) = x^{\langle p\rangle}(n), \quad n = 0, 1, \ldots, N-1, \\ &\widetilde{x} = \left[\widetilde{x}(0), \widetilde{x}(1), \ldots, \widetilde{x}(N-1)\right]^{T}. \end{aligned} \tag{8}$$

We divide $\widetilde{x}$ into M overlapping parts employing a real weighted function $h = [h(0), h(0), \ldots, h(L-1)]$; then the length of each part is L, and the shift length from part to part is S. The mth part of $\widetilde{x}$ can be written as

$$\widetilde{x}_m = \left[\widetilde{x}(mS), \widetilde{x}(mS+1), \ldots, \widetilde{x}(mS+L-1)\right]^{T}, \tag{9}$$

where $m = 0, 1, \ldots, M-1$. We define matrices $\mathbf{I}_L$ and $\boldsymbol{\Gamma}$ as

$$\begin{aligned} \mathbf{I}_L &= \begin{bmatrix} 1 & 1 & \cdots & 1 \\ 1 & 1 & \cdots & 1 \\ \vdots & \vdots & \ddots & \vdots \\ 1 & 1 & \cdots & 1 \end{bmatrix} \\ \boldsymbol{\Gamma} &= \begin{Bmatrix} [\mathbf{I}_L] & \cdots & \cdots & 0 \\ 0 \underset{\leftrightarrow}{\cdots} 0 & [\mathbf{I}_L] & \cdots & 0 \\ \vdots & \vdots & \ddots & \vdots \\ \underset{\leftarrow}{0} & \underset{(M-1)S}{\cdots} & \underset{\rightarrow}{0} & [\mathbf{I}_L] \end{Bmatrix}, \end{aligned} \tag{10}$$

where $\mathbf{I}_L$ is $L \times L$ identity matrix. $\boldsymbol{\Gamma}$ is a $ML \times N$ diagonal matrix, which is composed of M $\mathbf{I}_L$ elements; the shift distance between $\mathbf{I}_L$ and $\mathbf{I}_L$ is S. From (8) to (10), we can get the relationship between $\widetilde{x}$ and $\widetilde{x}_m$ as

$$\boldsymbol{\Gamma}\widetilde{x} = \left[\widetilde{x}_0^{T}, \widetilde{x}_1^{T}, \ldots, \widetilde{x}_{M-1}^{T}\right]^{T}. \tag{11}$$

We compute K ($K \geq L$) points discrete Fourier transform to (9) and obtain

$$\widetilde{X}_m = \left[\widetilde{X}_m(0), \widetilde{X}_m(1), \ldots, \widetilde{X}_m(K-1)\right]^T. \quad (12)$$

When all $\tilde{x}_m$ ($m = 0, 1, \ldots, M-1$) perform discrete Fourier transform, Fourier transform vector of $\tilde{x}$ is gotten:

$$\widetilde{X} = \left[\widetilde{X}_0^T, \widetilde{X}_1^T, \ldots, \widetilde{X}_{M-1}^T\right]^T. \quad (13)$$

We define $K \times K$ Fourier transform matrix $\mathbf{\Phi}$ as

$$\mathbf{\Phi} = \begin{bmatrix} 1 & e^{-j\omega_1} & \cdots & e^{-j(K-1)\omega_1} \\ 1 & e^{-j\omega_2} & \vdots & e^{-j(K-1)\omega_2} \\ \vdots & \vdots & \ddots & \vdots \\ 1 & e^{-j\omega_{K-1}} & \cdots & e^{-j(K-1)\omega_{K-1}} \end{bmatrix}. \quad (14)$$

And let

$$\mathbf{\Psi} = \begin{bmatrix} \longleftarrow & L & \longrightarrow & \\ 1 & 1 \cdots & 1 & \uparrow \\ \vdots & \vdots \vdots & \vdots & L \\ 1 & 1 \cdots & 1 & \downarrow \\ 0 & 0 \cdots & 0 & \uparrow \\ \vdots & \vdots \vdots & \vdots & K-L \\ 0 & 0 \cdots & 0 & \downarrow \end{bmatrix}. \quad (15)$$

$\mathbf{\Psi}$ is $K \times L$ ($K \geq L$) matrix. The weight function $h = [h(0), h(0), \ldots, h(L-1)]$ can be written as $L \times L$ diagonal matrix, as shown in

$$\mathbf{H} = \begin{bmatrix} h(0) & 0 & \cdots & 0 \\ 0 & h(1) & \vdots & 0 \\ \vdots & \vdots & \ddots & \vdots \\ 0 & 0 & \cdots & h(L-1) \end{bmatrix}. \quad (16)$$

By substituting (14)–(16) into (12), we can obtain

$$\widetilde{X}_m = \mathbf{\Phi\Psi H}\tilde{x}_m. \quad (17)$$

Similarly, (13) can be written as

$$\widetilde{X} = \begin{bmatrix} \mathbf{\Phi\Psi H} & 0 & \cdots & 0 \\ 0 & \mathbf{\Phi\Psi H} & 0 & \vdots \\ \vdots & 0 & \ddots & 0 \\ 0 & \cdots & 0 & \mathbf{\Phi\Psi H} \end{bmatrix} \begin{bmatrix} \tilde{x}_0 \\ \tilde{x}_1 \\ \vdots \\ \tilde{x}_{M-1} \end{bmatrix} = \left[\mathbf{I}_M \otimes (\mathbf{\Phi\Psi H})\right] \mathbf{\Gamma}\tilde{x} = \mathbf{B}\tilde{x}, \quad (18)$$

where $\mathbf{I}_M$ is $L \times L$ identity matrix, $\otimes$ denotes Kronecker tensor product, $(\mathbf{\Phi\Psi H})$ is $K \times L$ matrix, and $\mathbf{I}_M \otimes (\mathbf{\Phi\Psi H})$ is $(KM) \times (LM)$ matrix. $\mathbf{B} = [\mathbf{I}_M \otimes (\mathbf{\Phi\Psi H})]\mathbf{\Gamma}$, and $\mathbf{B}$ is $(KM) \times N$ matrix. We call (18) fractional low order short time Fourier transform (FLOSTFT).

3.3. Computation of Inverse FLOSTFT. In this section, we introduce how to solve fractional p order moments $\tilde{x}(n)$ of $x(n)$ from FLOSTFT. Both sides of (18) are multiplied $N \times KM$ matrix $\mathbf{\Gamma}^H[\mathbf{I}_M \otimes (\mathbf{\Psi}^H\mathbf{\Phi}^{-1})]$; we can get

$$\begin{aligned} &\mathbf{\Gamma}^H\left[\mathbf{I}_M \otimes \left(\mathbf{\Psi}^H\mathbf{\Phi}^{-1}\right)\right]\widetilde{X} \\ &= \mathbf{\Gamma}^H\left[\mathbf{I}_M \otimes \left(\mathbf{\Psi}^H\mathbf{\Phi}^{-1}\right)\right]\left[\mathbf{I}_M \otimes (\mathbf{\Phi\Psi H})\right]\mathbf{\Gamma}\tilde{x} \\ &= \mathbf{\Gamma}^H\left[(\mathbf{I}_M \cdot \mathbf{I}_M) \otimes \left(\mathbf{\Psi}^H\mathbf{\Phi}^{-1}\mathbf{\Phi\Psi H}\right)\right]\mathbf{\Gamma}\tilde{x} \\ &= \mathbf{\Gamma}^H\left[\mathbf{I}_M \otimes \left(\mathbf{\Psi}^H\mathbf{\Phi}^{-1}\mathbf{\Phi\Psi H}\right)\right]\mathbf{\Gamma}\tilde{x} \\ &= \mathbf{\Gamma}^H\left(\mathbf{I}_M \otimes \mathbf{H}\right)\mathbf{\Gamma}\tilde{x}. \end{aligned} \quad (19)$$

Then

$$\begin{aligned} \tilde{x}' &= \left[\mathbf{\Gamma}^H\left(\mathbf{I}_M \otimes \mathbf{H}\right)\mathbf{\Gamma}\right]^{-1}\mathbf{\Gamma}^H\left[\mathbf{I}_M \otimes \left(\mathbf{\Psi}^H\mathbf{\Phi}^{-1}\right)\right]\widetilde{X} \\ &= \mathbf{E}^{-1}\mathbf{\Lambda}\widetilde{X}, \end{aligned} \quad (20)$$

where $\tilde{x}'$ is the estimation of $\tilde{x}$. $\mathbf{E} = [\mathbf{\Gamma}^H(\mathbf{I}_M \otimes \mathbf{H})\mathbf{\Gamma}]^{-1}$ is $N \times N$ matrix, and $\mathbf{\Lambda} = \mathbf{\Gamma}^H[\mathbf{I}_M \otimes (\mathbf{\Psi}^H\mathbf{\Phi}^{-1})]$ is $N \times KM$ matrix. We call (20) inverse fractional low order short time Fourier transform (IFLOSTFT).

3.4. FLOSTFT-TFR Method. The squared magnitude of $\text{FLOSTFT}_x(t, f)$ in (7), denoted by $\text{FLOSTFT-TFR}_x(t, f)$, is

$$\begin{aligned} \text{FLOSTFT-TFR}_x(t, f) &= \left|\text{FLOSTFT}_x(t, f)\right|^2 \\ &= \left|\int_{-\infty}^{+\infty} x^{\langle p \rangle}(t)\, h(\tau - t)\, e^{-j2\pi f\tau} d\tau\right|^2. \end{aligned} \quad (21)$$

And the corresponding discrete form is written as

$$\begin{aligned} \text{FLOSTFT-TFR}_x(n, \omega) &= \left|\text{FLOSTFT}_x(n, \omega)\right|^2 \\ &= \left|\sum_m x^{\langle p \rangle}(m)\, h(m - n)\, e^{-j\omega n}\right|^2. \end{aligned} \quad (22)$$

Equations (21)-(22) are called fractional low order short time Fourier transform time-frequency representation (FLOSTFT-TFR). By solving (22), we can get time-frequency representation of $x(t)$.

4. FLOSTFT Time-Frequency Filtering Algorithm

Each signal has certain regions and feature in time-frequency domain. The problem is illustrated in Figure 2, which shows that the FM signals gather in the time regions from t_1 to t_2 and the frequency regions from f_1 to f_2. Then, we can separate the signal from the noise or eliminate undesired parts of the signal in time-frequency domain. In this section, we will study the time-frequency filtering algorithm based on the ISTFT and IFLOSTFT method under α stable distribution noise.

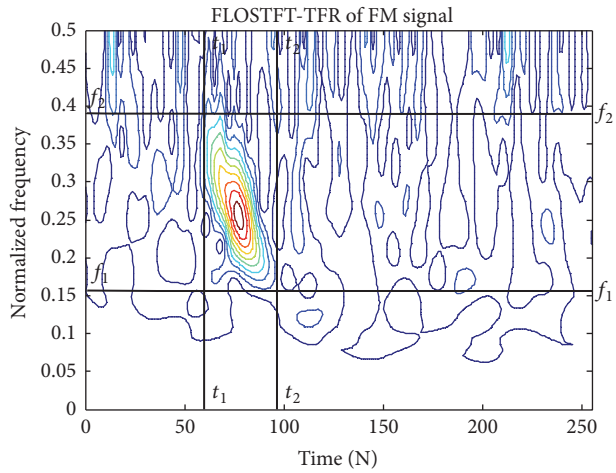

Figure 2: Time-frequency representation of FM signal employing the FLOSTFT-TFR method under α stable distribution noise.

4.1. STFT-TFF Algorithm. Short time Fourier transform (STFT) of $x(t)$ is defined as

$$\text{STFT} = \int_{-\infty}^{+\infty} x(t)\, h(\tau - t)\, e^{-j2\pi f\tau} d\tau. \tag{23}$$

And the corresponding short time Fourier transform time-frequency representation (STFT-TFR) is expressed as

$$\begin{aligned}\text{STFT-TFR}_x(t, f) &= \left|\text{STFT}_x(t, f)\right|^2 \\ &= \left|\int_{-\infty}^{+\infty} x(t)\, h(\tau - t)\, e^{-j2\pi f\tau} d\tau\right|^2.\end{aligned} \tag{24}$$

When both sides of (24) are multiplied by a weight function $F(t, f)$, we have

$$\begin{aligned}\text{STFT-TFR}'_x(t, f) &= \text{STFT-TFR}_x(t, f)\, F(t, f) \\ &= \left|\text{STFT}_x(t, f)\right|^2 F(t, f).\end{aligned} \tag{25}$$

$F(\tau, f)$ is designed according to time and frequency characteristics of the signal in time domain. From (25), we calculate inverse transform, yielding

$$\begin{aligned}\text{STFT}'_x(t_i, f_q) = &\sqrt{\left|\text{STFT-TFR}'_x(t_i, f_q)\right|} \\ &\cdot \text{sign}\left[\text{STFT}_x(t_i, f_q)\right],\end{aligned} \tag{26}$$

where $\text{STFT}'_x(t_i, f_q)$ is the estimation of $\text{STFT}_x(t_i, f_q)$, which is filtered by the filtering function $F(\tau, f)$ in time-frequency domain. When all $\text{STFT}'_x(t_i, f_q)$ is solved, we obtain $\text{STFT}'_x(t, f)$. Following, we can calculate its inverse STFT employing the method in [19], and the estimated $x'(t)$ is gotten. The time-frequency filtering method is called short time Fourier transform time-frequency filtering (STFT-TFF) algorithm.

4.2. FLOSTFT-TFF Algorithm. The STFT-TFR method fails under α stable distribution noise environment, and the STFT-TFF time-frequency filtering method based on the STFT-TFR method degenerates; hence, the FLOSTFT-TFR method has been demonstrated in Section 3. In this section, we will study how to restore the signal from its time-frequency representation employing the FLOSTFT-TFR method.

We multiply a weight function $F(t, f)$ on both sides of (21) and then obtain

$$\begin{aligned}&\text{FLOSTFT-TFR}'_x(t, f) \\ &\quad= \text{FLOSTFT-TFR}_x(t, f)\, F(t, f) \\ &\quad= \left|\text{FLOSTFT}_x(t, f)\right|^2 F(t, f).\end{aligned} \tag{27}$$

$F(\tau, f)$ is a filter function, which is selected according to time-frequency characteristics of the signal. We define the estimation of $\text{FLOSTFT}_x(t, f)$ as

$$\begin{aligned}\text{FLOSTFT}'_x(t_i, f_q) = &\sqrt{\left|\text{FLOSTFT-TFR}'_x(t_i, f_q)\right|} \\ &\cdot \text{sign}\left[\text{FLOSTFT}_x(t_i, f_q)\right],\end{aligned} \tag{28}$$

where (t_i, f_q) is ith time point and qth frequency point. When all points $\text{FLOSTFT}'_x(t_i, f_q)$ are calculated, we can obtain $\text{FLOSTFT}'_x(t, f)$. Then, we can solve $\widetilde{x}(t)$ employing the IFLOSTFT method in Section 3.3. For the real signal $x(t)$, we have

$$\widetilde{x}(t) = x^{\langle p\rangle}(t) = |x(t)|^{p-1} \cdot \text{sign}[x(t)]. \tag{29}$$

From (29), we obtain

$$\widehat{x}(t) = \left|\widetilde{x}'(t)\right|^{1/(p-1)} \text{sign}\left[\widetilde{x}'(t)\right]. \tag{30}$$

$\widetilde{x}'(t)$ in (30) is the estimation of $x(t)$. We call the filtering method fractional low order short time Fourier transform time-frequency filtering (FLOSTFT-TFF) algorithm.

4.3. FLOSTFT-TFF Algorithm Steps

Step 1. Calculate FLOSTFT with (6).

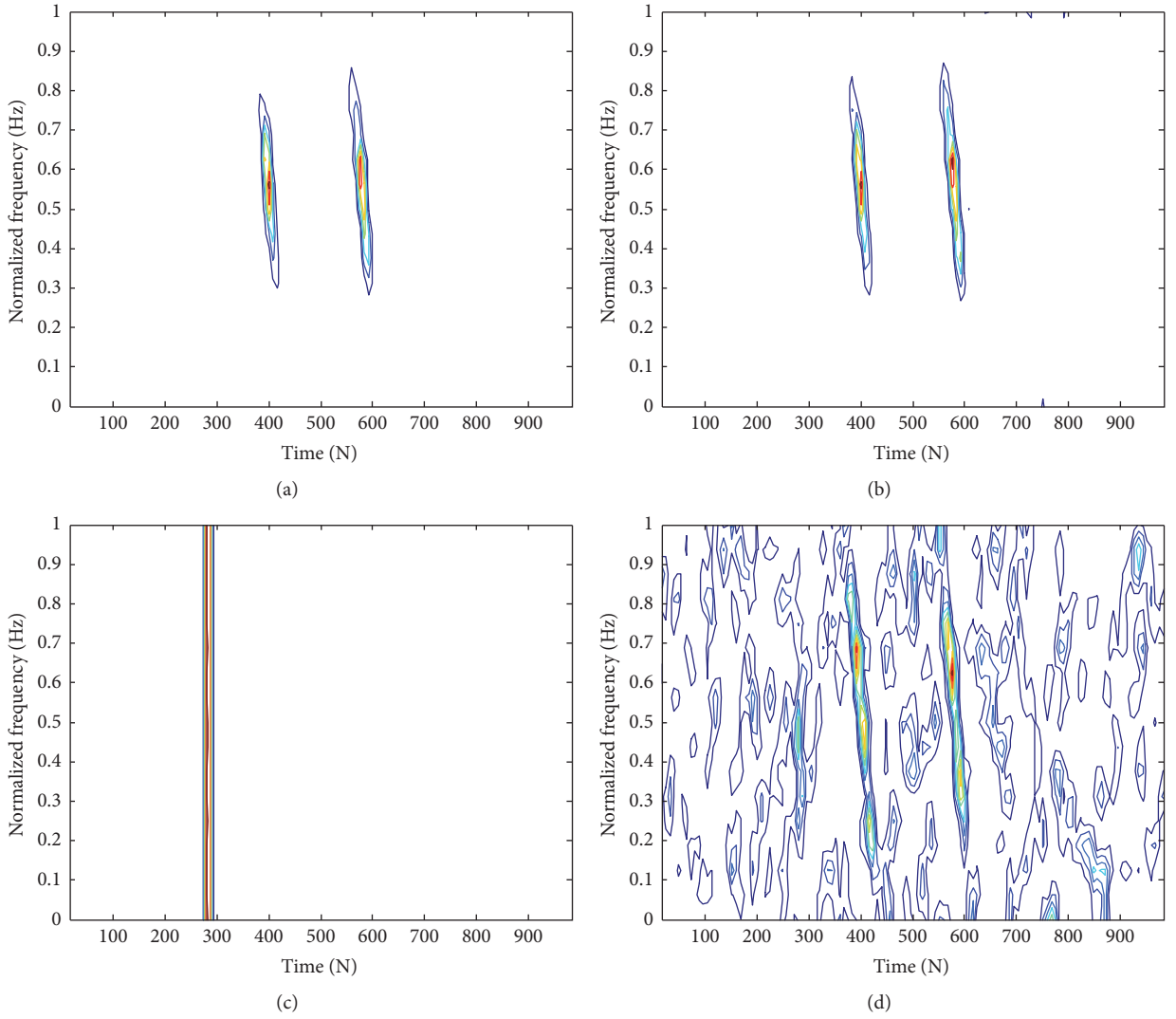

Figure 3: Time-frequency distributions of $x(n)$ employing the STFT-TFR and FLOSTFT-TFR methods. (a) Time-frequency distribution employing the STFT-TFR method under Gaussian noise environment. (b) Time-frequency distribution employing the FLOSTFT-TFR method under Gaussian noise environment. (c) Time-frequency distribution employing the STFT-TFR method under SαS distribution noise environment. (d) Time-frequency distribution employing the FLOSTFT-TFR method under SαS distribution noise environment.

Step 2. Compute FLOSTFT-TFR employing (21).

Step 3. Select appropriate filter function $F(\tau, f)$ and extract the time-frequency regions of the signal employing (27).

Step 4. Calculate inverse FLOSTFT-TFR with (28), and compute IFLOSTFT employing (19)-(20).

Step 5. Perform inverse operation of $\widetilde{x}'(t)$ with (30).

5. Simulations

The real signal $y(n)$ contaminated by the noise may be written as

$$y(n) = x(n) + v(n). \tag{31}$$

And two FM signals are expressed as

$$\begin{aligned} x_1(n) &= e^{-a(n-N_1)^2 + jc(n-N_1)^2 + j\omega(n-N_1)} \\ x_2(n) &= e^{-a(n-N_2)^2 + jc(n-N_2)^2 + j\omega(n-N_2)}, \end{aligned} \tag{32}$$

where $a = 0.004$, $c = -0.025$, $\omega = 1.72$, $N_1 = 420$, $N_2 = 560$, and $v(t)$ is Gaussian noise or α stable distribution noise. We let $x(n) = \text{real}[x_1(n)] + \text{real}[x_2(n)]$, $n = 0, 1, 2, \ldots, N-1$. When $v(t)$ is Gaussian noise, signal to noise ratio (SNR) can be used, however. If $v(t)$ is α stable distribution noise, SNR is unusable. Hence, we apply generalized signal noise ratio (GSNR) to substitute SNR, and GSNR $= 10\log_{10}\{E[|x(n)|^2]/\gamma^\alpha\}$. To measure the

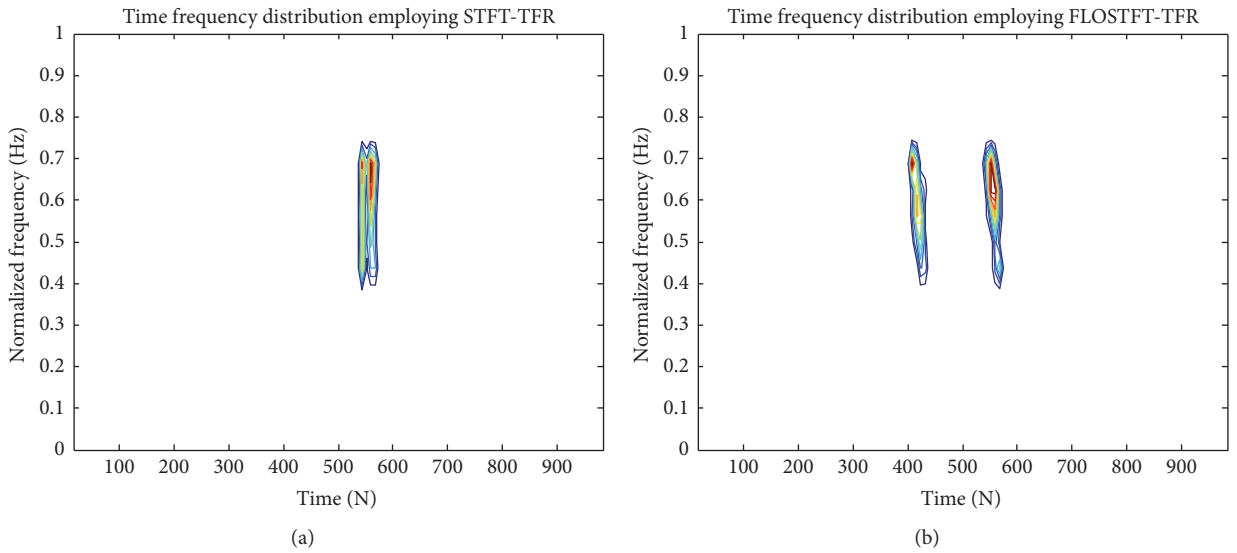

Figure 4: The filtered time-frequency representation employing the STFF-TFF and FLOSTFT-TFF method under SαS distribution noise environment. (a) Time-frequency representation of $x(n)$ filtered by the STFF-TFF method. (b) Time-frequency representation of $x(n)$ filtered by the FLOSTFF-TFF method.

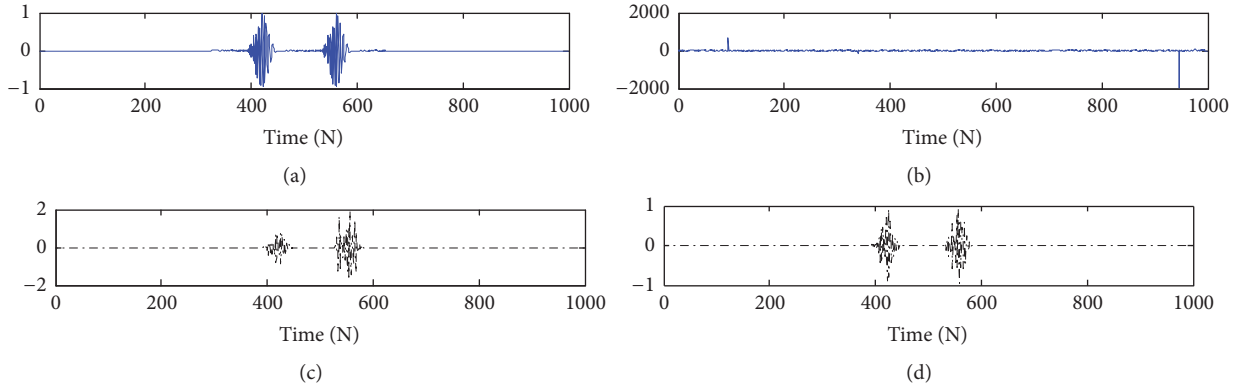

Figure 5: The real waveforms of two FM signals in time domain. (a) The original signal. (b) The original signal contaminated by SαS distribution noise. (c) The estimated signal employing the STFT-TFF method. (d) The estimated signal employing the FLOSTFT-TFF method.

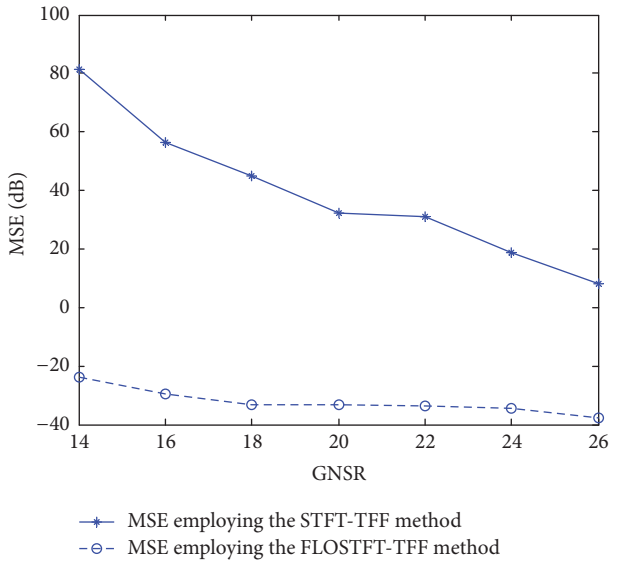

Figure 6: The mixed MSEs employing the STFT-TFF and FLOSTFT-TFF methods under different GSNR (14 dB–26 dB).

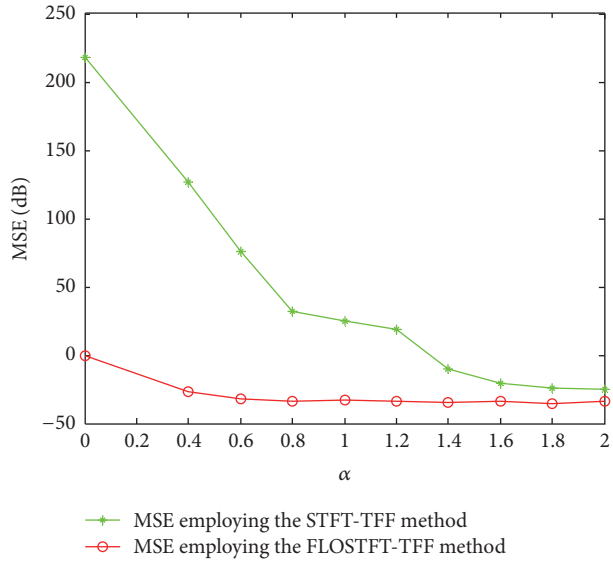

Figure 7: The mixed MSEs employing the STFT-TFF and FLOSTFT-TFF methods under different α (0–2).

performance of the proposed methods, we define mixed mean square error (MSE) as

$$\text{MSE} = \frac{1}{K}\sum_{k=1}^{K}\left\{\frac{1}{N}\sum_{n=1}^{N}\left[\hat{x}_1(n) - x_1(n)\right]^2 + \frac{1}{N}\sum_{n=1}^{N}\left[\hat{x}_2(n) - x_2(n)\right]^2\right\}, \tag{33}$$

where K is the number of Monte-Carlo experiments and $\hat{x}_1(n)$ and $\hat{x}_2(n)$ denote the signals estimated by the STFT-TFF or FLOSTFT-TFF methods.

5.1. Study of the FLOSTFT-TFR and STFT-TFR Methods. In this simulation, we apply the FLOSTFT-TFR and STFT-TFR methods to demonstrate the time-frequency distribution of FM signals under Gaussian noise and SαS stable distribution noise environment, respectively. If $v(n)$ is Gaussian noise ($\alpha = 2$), we set SNR = 12 dB, $p = 1.8$. And if $v(n)$ is SαS distribution noise, we set the characteristic index of SαS distribution noise $\alpha = 0.8$, fractional low order moment parameter $p = 1.1$, GSNR = 16 dB, and length of the weighted function $L = 32$. The experimental results are shown in Figures 3(a)–3(d).

Figures 3(a) and 3(b) are the time-frequency distributions of $x(n)$ employing the STFT-TFR and FLOSTFT-TFR methods under Gaussian noise environment, respectively. The figures show that the methods can also obtain time-frequency distribution of $x(n)$. Time-frequency distributions of $x(n)$ employing the STFT-TFR and FLOSTFT-TFR methods under α stable distribution noise environment are shown in Figures 3(c) and 3(d), respectively. The results show that the STFT-TFR method fails, and the FLOSTFT-TFR method has good performance. Hence, the FLOSTFT-TFR method has better performance in demonstrating the time-frequency distribution of the signals than the STFT-TFR method under α stable distribution noise environment and is robust.

5.2. Study of the FLOSTFT-TFF and STFT-TFF Algorithm. In this simulation, we set $v(n)$ as SαS distribution noise, $\alpha = 0.8$, $p = 1.2$, GSNR = 18 dB, and $L = 32$. We apply the FLOSTFT-TFF and STFT-TFF methods to reconstruct the original FM signals from SαS distribution noise; the simulations are shown in Figure 4.

Figures 4(a) and 4(b) are the time-frequency representations of $x(n)$ filtered by the STFF-TFF and FLOSTFF-TFF methods under SαS distribution noise environment, respectively. The results show that the time-frequency representation filtered by the STFF-TFF method is incorrect, but the FLOSTFF-TFF method can better extract the time-frequency distribution of $x(n)$. Hence, the FLOSTTF-TFF method has better performance in extracting time-frequency distribution of the signal under SαS distribution noise environment.

In Figure 5 we show from (a) to (d) the original FM signal, the original FM signal contaminated by SαS distribution noise, the estimated FM signal employing the STFT-TFF method, and the FM signal estimated by the FLOSTFT-TFF method. The experimental results show that the contaminated original signal is overwhelmed by SαS distribution noise. The restored signal employing the STFT-TFF method has larger deviation, but the signal reconstructed by the FLOSTFT-TFF method is similar to the original signal. Hence, the FLOSTFT-TFF method has a better quality of signal reconstruction under α stable distribution noise environment.

5.3. MSE Analysis under Different α and GSNR. In this simulation, $v(n)$ is set as SαS distribution noise, $\alpha = 0.8$, $p = 1.2$, GSNR = 18 dB, and $L = 32$. We apply the FLOSTFT-TFF and STFT-TFF methods to restore the original FM signals and

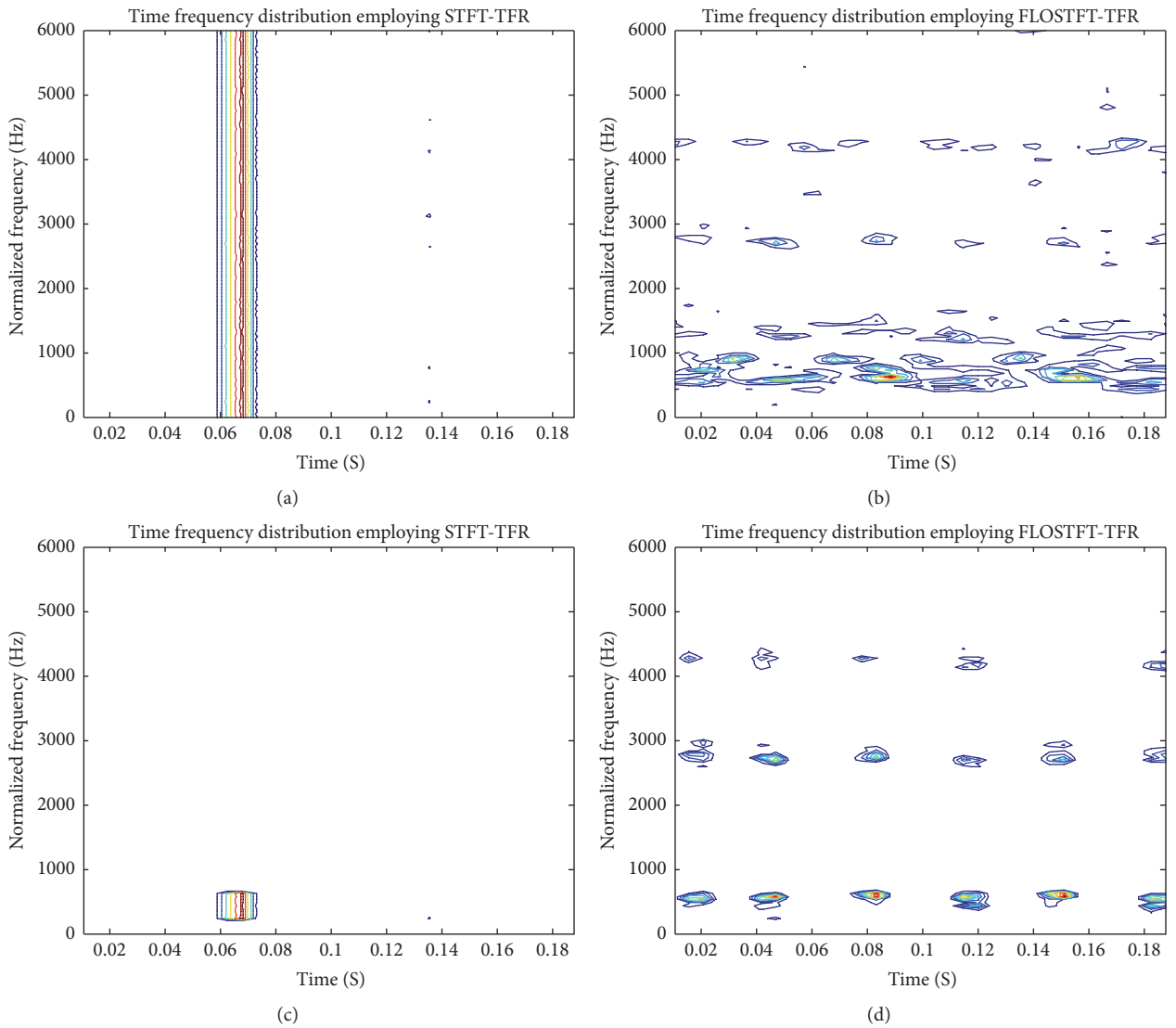

Figure 8: Time-frequency representations of the machine fault signals in BA under SαS distribution noise environment. (a) Time-frequency representation of the machine fault signals in BA employing the STFT-TFR. (b) Time-frequency representation of the machine fault signals in BA employing the FLOSTFT-TFR. (c) The machine fault signals in BA restored by the STFT-TFF method. (d) The fault signals in BA reconstructed by the FLOSTFT-TFF method.

compare MSEs of the methods under different GSNR and α; the simulations are shown in Figures 6 and 7.

Figure 6 is MSE analysis under different GSNR; the experimental results show that MSEs employing the STFT-TFF method vary from 8 dB to 80 dB when GSNR change from 26 dB to 14 dB, but MSEs employing the FLOSTFT-TFF method are in the range of −20 dB to −40 dB. Hence, the FLOSTFT-TFF method has obvious advantage to restore the original signals under different GSNR. In particular, the advantage of the FLOSTFT-TFF method is more obvious when GSNR < 18 dB.

The MSE analysis of the STFT-TFF and FLOSTFT-TFF methods under different α is shown in Figure 7. We see that MSEs of the STFT-TFF method have a large variation, which vary from −20 dB to 220 dB, but MSE of the FLOSTFT-TFF method is stable about −30 dB. Hence, the FLOSTFT-TFF method has better stability in reconstructing the original signals.

5.4. Applications of FLOSTFT-TFF Method to Machine Fault Signals. In this simulation, the experiment signal is adopted from the Case Western Reserve University (CWRU) bearing data center [33]. The faulted bearings with fault diameters of 0.007 inches are reinstalled into the test motor, and the motor speed is 1797 RPM (revolutions per minute). The digital data is collected at 12,000 samples per second, and 0.2-second data is selected as test signal from the outer race bearing fault in BA, DE, and FE; then $N = 2400$. SαS distribution noise ($\alpha = 0.8$, GSNR = 15 dB) is added in the fault signals, which is assumed as the actual working environment

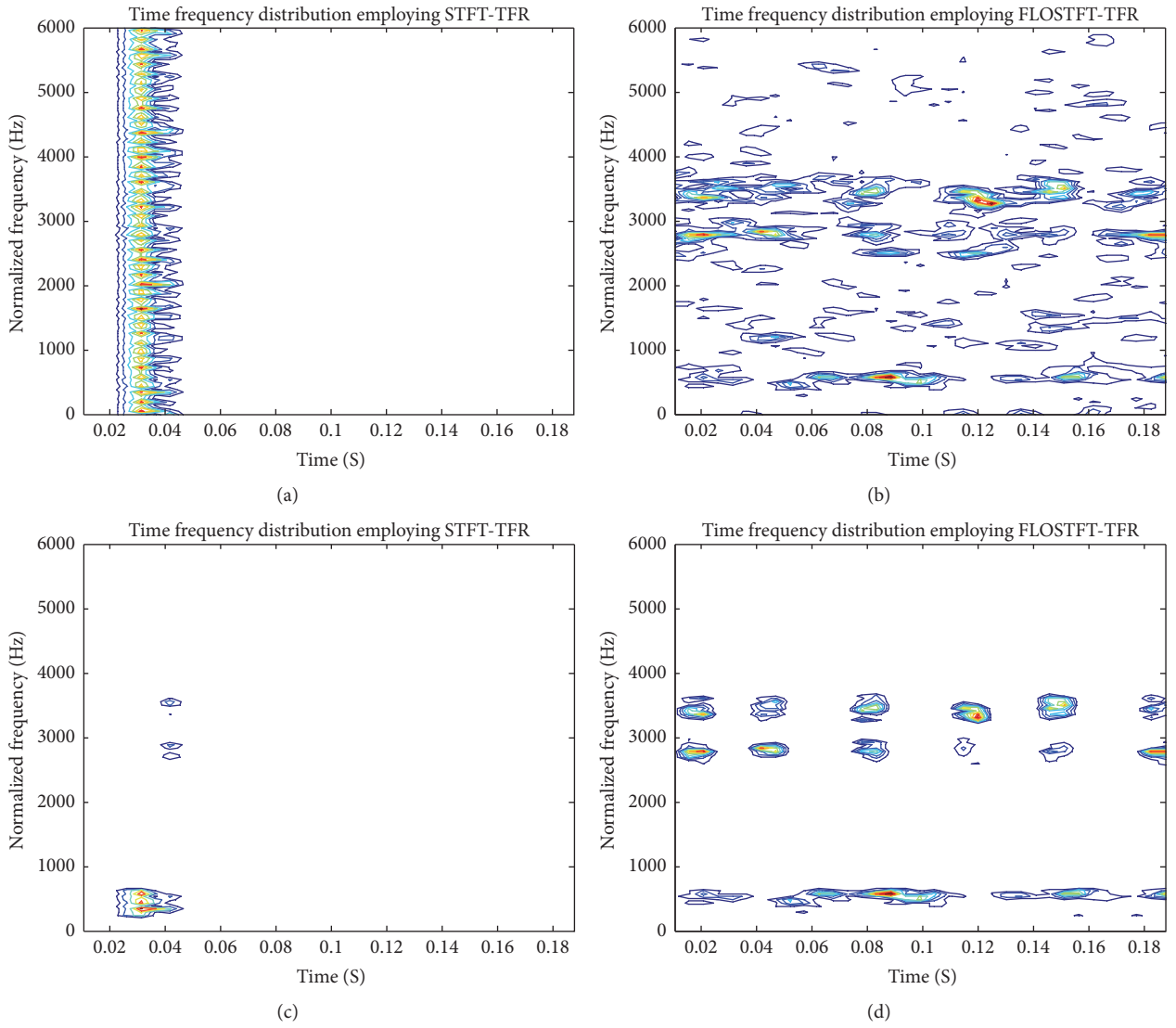

Figure 9: Time-frequency representations of the machine fault signals in DE under SαS distribution noise environment. (a) Time-frequency representation of the machine fault signals in DE employing the STFT-TFR method. (b) Time-frequency representation of the machine fault signals in DE employing the FLOSTFT-TFR method. (c) The machine fault signals in DE restored by the STFT-TFF method. (d) The fault signals in DE reconstructed by the FLOSTFT-TFF method.

background noise. The STFT-TFR and FLOSTFT-TFR methods are used to demonstrate time-frequency distribution of the fault signals for fault analysis. Similarly, the STFT-TFF and FLOSTFT-TFF methods are also applied to restore the original bearing outer race fault signals from SαS distribution noise. The experimental simulations are shown in Figures 8–13.

Figures 8(a) and 8(b) are time-frequency distributions of the bearing outer race fault signal in BA employing the STFT-TFR and FLOSTFT-TFR methods, respectively. The STFT-TFR and FLOSTFT-TFR time-frequency distributions of the bearing outer race fault signals in DE and FE are shown in Figures 9(a), 10(a), 9(b), and 10(b), respectively. The figures show that the STFT-TFR method fails, but the FLOSTFT-TFR method can better demonstrate the time-frequency representations of the bearing outer race fault signals, which has good performance.

Figures 8(c)-10(c) and Figures 8(d)-10(d) are the time-frequency distributions filtered by the STFT-TFF and FLOSTFT-TFF methods, respectively. In the figures, we see that the extracted time-frequency representations employing the STFF-TFF method are incorrect, as shown in Figures 8(c)-10(c). But the FLOSTFT-TFF method in Figures 8(d)-10(d) can better fetch the time-frequency distribution of the fault signals. In Figures 8(d)-10(d) we may know that the gap regularly changes between the impacts, the fault vibration interval is approximately 30 ms, and the interval corresponds to the characteristic frequency of outer race which is 33.33 Hz. In Figure 8(d) the shock pulse is mainly distributed in low-frequency band from 500 Hz to 4500 Hz, and the transient

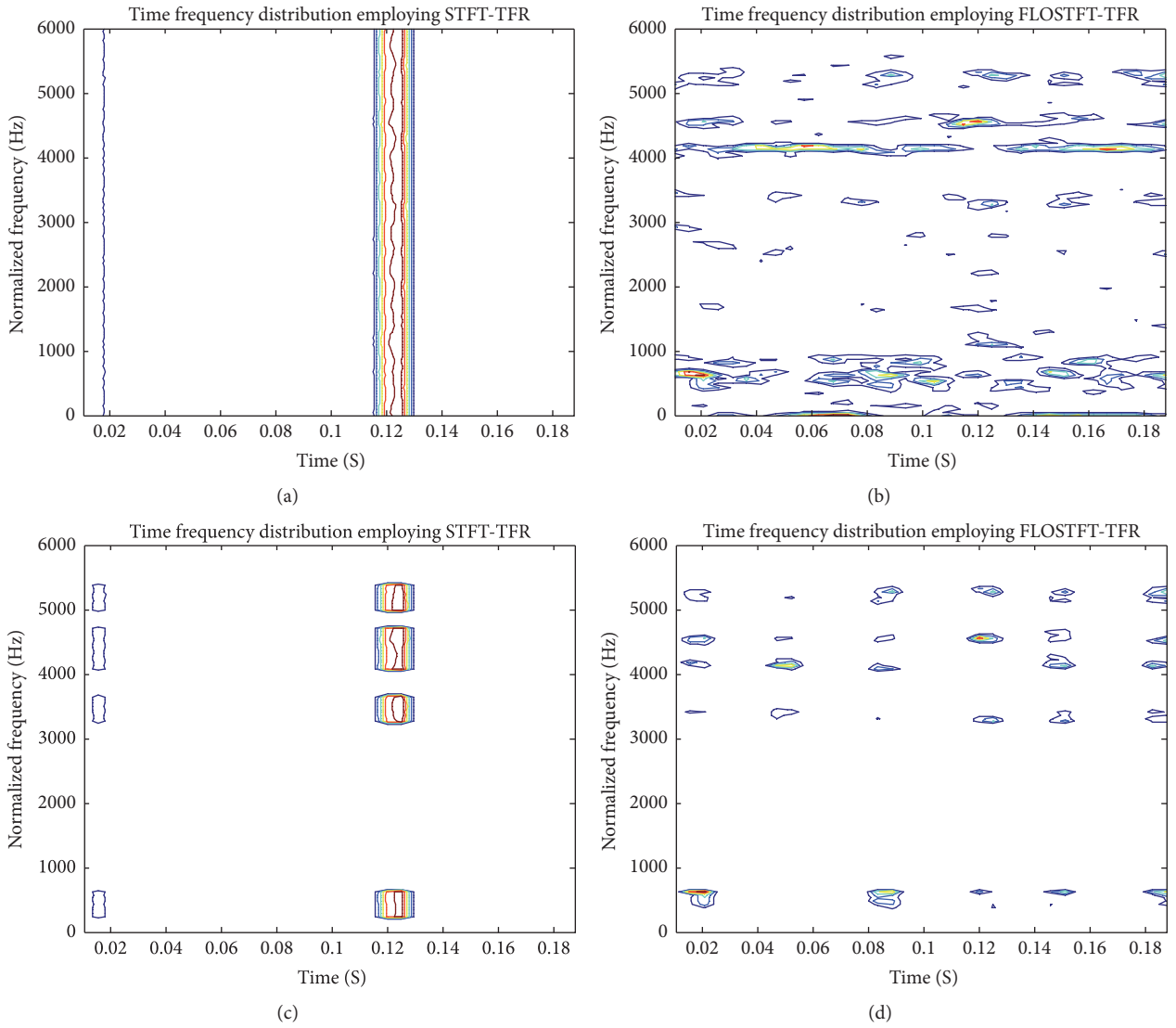

FIGURE 10: Time-frequency representations of the machine fault signals in FE under SαS distribution noise environment. (a) Time-frequency representation of the machine fault signals in FE employing the STFT-TFR method. (b) Time-frequency representation of the machine fault signals in FE employing the FLOSTFT-TFR method. (c) The machine fault signals in FE restored by the STFT-TFF method. (d) The fault signals in FE reconstructed by the FLOSTFT-TFF method.

harmonic vibration components of about 600 Hz, 2800 Hz, and 4200 Hz dominate frequency-domain. In Figure 9(d) the transient harmonic vibration components are about 600 Hz, 2800 Hz, and 4200 Hz, and the transient harmonic vibration components of about 600 Hz, 3400 Hz, 4500 Hz, and 5200 Hz are shown in Figure 10(d).

In Figures 11–13 we show from (a) to (d) the waveforms of the original bearing outer race fault signals in BA, DE, and FE, the original bearing outer race fault signals contaminated by SαS distribution noise, the bearing outer race fault signals reconstructed by the STFT-TFF method, and the reconstructed bearing outer race fault signals employing the FLOSTFT-TFF method, respectively. The simulations show that the contaminated bearing outer race fault signals in BA, DE, and FE are overwhelmed by SαS distribution noise in Figures 11(b)-13(b), the restored outer race fault signals employing the STFT-TFF method have larger deviation in Figures 11(c)-13(c), and the reconstructed outer race fault signals employing the FLOSTFT-TFF method are similar to the original signal in Figures 11(d)-13(d), respectively. Hence, the FLOSTFT-TFF method has a better quality of signal recovery for the bearing outer race fault signals.

Combined with the results of upper experiments, we see that the FLOSTFT-TFF method can better demonstrate time-frequency distribution of the machine fault signals and extract their fault features than the existing STFT-TFF method under SαS distribution noise environment.

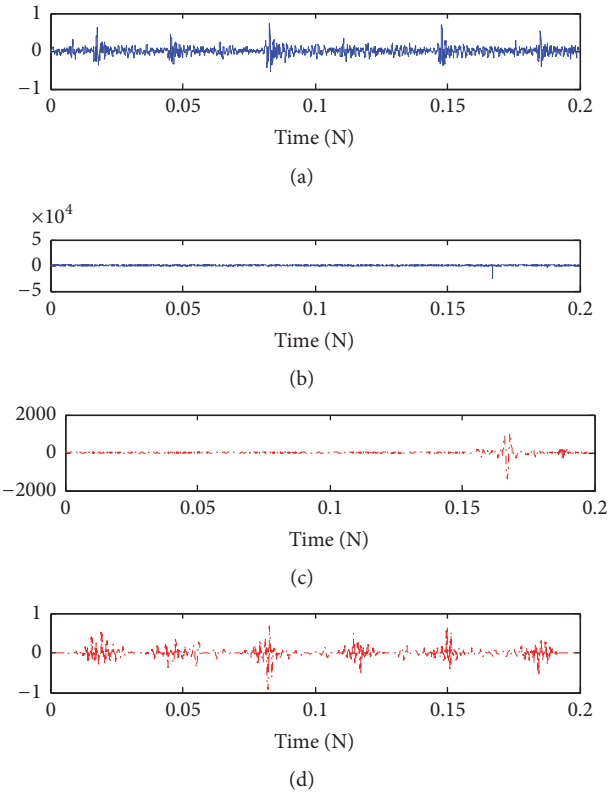

Figure 11: The waveforms of the machine fault signals in time domain. (a) The original bearing out race fault signals in BA. (b) The original bearing outer race fault signals in BA contaminated by SαS distribution noise. (c) The restored bearing outer race fault signals in BA employing the STFT-TFF method. (d) The bearing outer race fault signals in BA resconstructed by the FLOSTFT-TFF method.

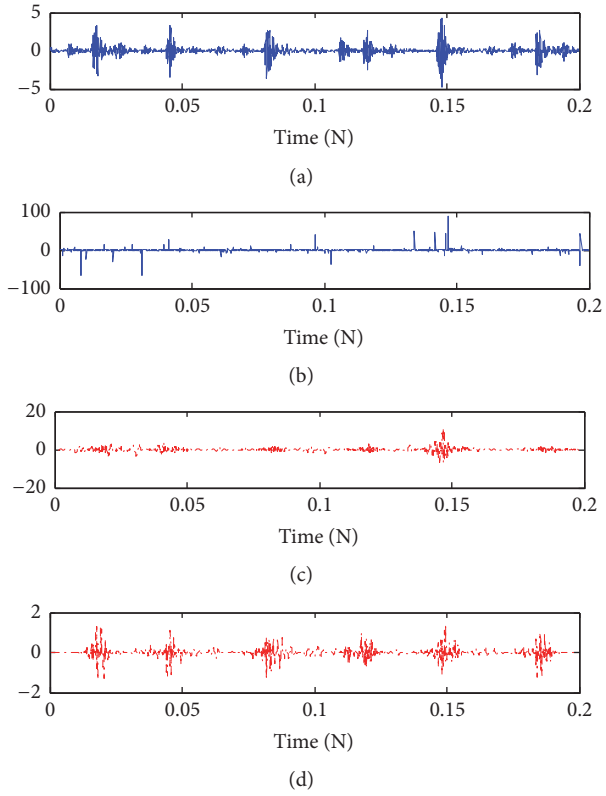

Figure 12: The waveforms of the machine fault signals in time domain. (a) The original bearing outer race fault signals in DE. (b) The original bearing outer race fault signals in DE contaminated by SαS distribution noise. (c) The restored bearing outer race fault signals in DE employing the STFT-TFF method. (d) The bearing outer race fault signals in DE reconstructed by the FLOSTFT-TFF method.

6. Discussion

(i) Fractional p order moment $x^{\langle p \rangle}(t)$ of the nonstationary signal $x(t)$ is stationary and integrable within the time window $h(t)$; however, the traditional STFT method is still no-stationary and integrable because when $\alpha < 1$, $E[|s|] = \infty$.

(ii) The shorter the length of weight function L, the higher time resolution, but the lower the frequency resolution. In a practical application, we should set a reasonable balance value between time resolution and frequency resolution and select the proper length of window function.

(iii) We can set the parameter p according to characteristic index of α stable distribution noise α; the smaller α, the smaller p. When $p = 2$, the FLOSTFT method degenerates into the STFT method, and the corresponding IFLOSTFT evolves into the ISTFT method,;hence, the improved FLOSTFT is a generalized algorithm.

(iv) The FLOSTFT and IFLOSTFT methods are a linear transformation, but the FLOSTFT-TFR algorithm is a nonlinear transformation.

7. Conclusions

In this paper, we consider α stable distribution noise as the background noise. Hence, the improved FLOSTFT and IFLOSTFT methods employing fractional p order moment are proposed, and FLOSTFT-TFR is presented for time-frequency analysis. We take advantage of time-frequency localized spectra of the signal and propose a novel FLOSTFT-TFF method, which can restore the original signal from α stable distribution noise. We apply the FLOSTFT-TFR method to get time-frequency distribution of two FM signals and use the FLOSTFT-TFF method to extract the time-frequency distribution of two FM signals from SαS distribution noise; finally, the IFLOSTFT algorithm is used to restore the original FM signals; the results demonstrate their effectiveness. We compare the performance of the STFT-TFF and FLOSTFT-TFF methods; the results show that the performance of the FLOSTFT-TFF method is better than the STFT-TFF method, which can effectively suppress SαS distribution noise and work in low GSNR. In practical applications, we analyze the fault features from time-frequency representation of the mechanical bearing fault signals employing FLOSTFT-TFR method, extract time-frequency region of the fault signals

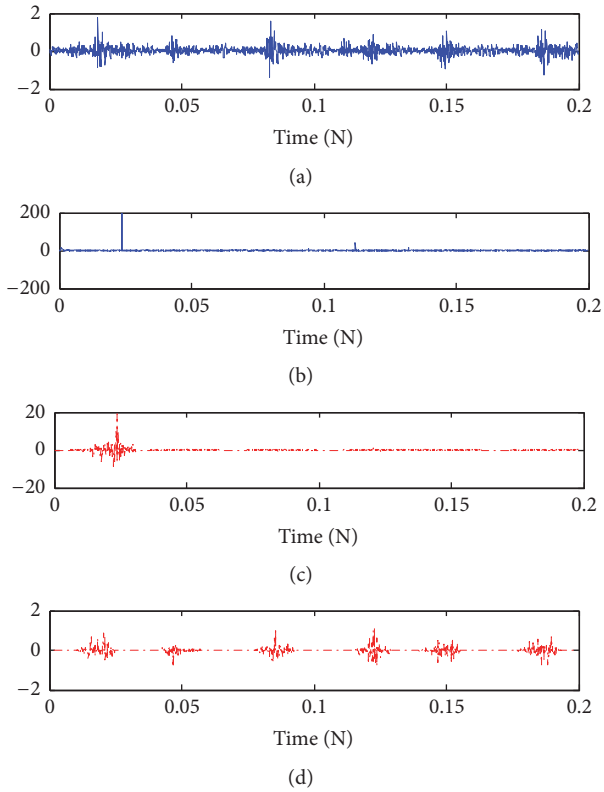

Figure 13: The waveforms of the machine fault signals in time domain. (a) The original bearing outer race fault signals in FE. (b) The original bearing outer race fault signals in FE contaminated by SαS distribution noise. (c) The restored bearing outer race fault signals in FE employing the STFT-TFF method. (d) The bearing outer race fault signals in FE reconstructed by the FLOSTFT-TFF method.

from α stable distribution noise employing FLOSTFT-TFF method, and reconstruct the original fault signal employing IFLOSTFT.

Conflicts of Interest

The authors declare that they have no conflicts of interest.

Acknowledgments

This work is financially supported by Natural Science Foundation of China (61261046 and 61362038), the Natural Science Foundation of Jiangxi Province, China (20142BAB207006 and 20151BAB207013), the Research Foundation of Health Department of Jiangxi Province, China (20175561), and Science and Technology Project of Jiujiang University, China (2013KJ01, 2016KJ001, 2016KJ002, and 2016KJ003).

References

[1] T. Higuchi, N. Ito, T. Yoshioka, and T. Nakatani, "Robust MVDR beamforming using time-frequency masks for online/offline ASR in noise," in *Proceeding of the 41st IEEE International Conference on Acoustics, Speech and Signal Processing (ICASSP '16)*, pp. 5210–5214, China, March 2016.

[2] X. Wang, Y. Zheng, Z. Zhao, and J. Wang, "Bearing fault diagnosis based on statistical locally linear embedding," *Sensors*, vol. 15, no. 7, pp. 16225–16247, 2015.

[3] A. Katunin, "Application of time-frequency distributions in diagnostic signal processing problems: a case study," *Diagnostyka*, vol. 17, no. 2, pp. 95–103, 2016.

[4] A. S. Alfahoum and A. Alfraihat, "Methods of EEG Signal Features Extraction Using Linear Analysis in Frequency and Time-Frequency Domains," *Isrn Neuroscience*, vol. 2014, no. 3, Article ID 730218, 2014.

[5] N. H. Chandra, A. S. Sekhar, N. H. Chandra et al., "Fault detection in rotor bearing systems using time frequency techniques," *Mechanical Systems & Signal Processing*, vol. 72-73, pp. 105–133, 2015.

[6] Y. Andrianakis and P. R. White, "A speech enhancement algorithm based on a chi mrf model of the speech STFT amplitudes," *IEEE Transactions on Audio Speech & Language Processing*, vol. 17, no. 8, pp. 1508–1517, 2009.

[7] M. Krawczyk and T. Gerkmann, "STFT phase reconstruction in voiced speech for an improved single-channel speech enhancement," *IEEE/ACM Transactions on Audio Speech & Language Processing*, vol. 22, no. 12, pp. 1931–1940, 2014.

[8] S. Aldirmaz and L. Durak, "Broadband interference excision in spread spectrum communication systems based on short-time fourier transformation," *Pier B*, vol. 7, pp. 309–320, 2008.

[9] S. Aldırmaz and L. Durak, "Performance analysis of an STFT-based broadband interference excision algorithm in DS-SS systems," in *Proceeding of Siu IEEE 15th Signal Processing & Communications Applications*, pp. 1–4, June 2007.

[10] A. R. Abdullah, N. S. Ahmad, N. H. Bahari et al., "Switched Faults Analysis of Voltage Source Inverter (VSI) using Short Time Fourier Transform (STFT)," *International Review on Modelling & Simulations*, vol. 7, no. 3, pp. 409–415, 2014.

[11] H. Zhang, G. Bi, Y. Cai, S. G. Razul, and C. M. S. See, "DOA estimation of closely-spaced and spectrally-overlapped sources using a STFT-based MUSIC algorithm," *Digital Signal Processing: A Review Journal*, vol. 52, pp. 25–34, 2016.

[12] M. Schimmel and J. Gallart, "Authors' Reply to Comments on 'The Inverse S-Transform in Filters With Time-Frequency Localization'," *IEEE Transactions on Signal Processing*, vol. 55, no. 10, pp. 5120–5121, 2007.

[13] M. Schimmel and J. Gallart, "The inverse S-transform in filters with time-frequency localization," *IEEE Transactions on Signal Processing*, vol. 53, no. 11, pp. 4417–4422, 2005.

[14] D. Wang, J. Wang, Y. Liu et al., "An adaptive time-frequency filtering algorithm for multi-component LFM signals based on generalized S-transform," in *Proceeding of the International Conference on Automation & Computing*, Glasgow UK, September 2015.

[15] J. Wang, Y. G. He, G. F. Fang et al., "NWST and TT transform joint time-frequency filtering," *Application Research of Computers*, vol. 29, no. 11, pp. 4254–4256, 2012.

[16] X. H. Chen, H. E. Zhen, and D. J. Huang, "Generalized S Transform and its time-frequency filtering," *Signal Processing*, vol. 24, no. 1, pp. 28–31, 2008.

[17] H. S. Chi, H. X. Wang, Q. Guo et al., "Application of STFT in time frequency filtering of lfm signals," *Telecommunication Engineering*, vol. 52, no. 2, pp. 155–159, 2012.

[18] Z. Zha and X. Shi, "FM interference suppression based on STFT and time varying filtering," *Journal of Detection & Control*, vol. 31, no. 3, pp. 46–50, 2009.

[19] B. Yang, "A study of inverse short-time fourier transform," in *Proceeding of the IEEE International Conference on Acoustics, Speech and Signal Processing (ICASSP '08)*, pp. 3541–3544, Las Vegas, NV, USA, April 2008.

[20] X. Ma and C. L. Nikias, "Joint estimation of time delay and frequency delay in impulsive noise using fractional lower order statistics," *IEEE Transactions on Signal Processing*, vol. 44, no. 11, pp. 2669–2687, 1996.

[21] M. Shao and C. L. Nikias, "Signal processing with fractional lower order moments: stable processes and their applications," *Proceedings of the IEEE*, vol. 81, no. 7, pp. 986–1010, 1993.

[22] X. Ma and C. L. Nikias, "Parameter estimation and blind channel identification in impulsive signal environments," *IEEE Transactions on Signal Processing*, vol. 43, no. 12, pp. 2884–2897, 1995.

[23] T.-H. Liu and J. M. Mendel, "A subspace-based direction finding algorithm using fractional lower order statistics," *IEEE Transactions on Signal Processing*, vol. 49, no. 8, pp. 1605–1613, 2001.

[24] L. R. Padovese, "Hybrid time-frequency methods for non-stationary mechanical signal analysis," *Mechanical Systems and Signal Processing*, vol. 18, no. 5, pp. 1047–1064, 2004.

[25] A. G. Poulimenos and S. D. Fassois, "Parametric time-domain methods for non-stationary random vibration modelling and analysis—a critical survey and comparison," *Mechanical Systems and Signal Processing*, vol. 20, no. 4, pp. 763–816, 2006.

[26] J. B. Long and H. B. Wang, "Parameter estimation and time-frequency distribution of fractional lower order time-frequency auto-regressive moving average model algorithm based on SαS process," *Journal of Electronics & Information Technology*, vol. 38, no. 7, pp. 1710–1716, 2016.

[27] C. Li and G. Yu, "A new statistical model for rolling element bearing fault signals based on alpha-stable distribution," in *Proceeding of the International Conference on Computer Modeling and Simulation (ICCMS '10)*, pp. 386–390, China, January 2010.

[28] X. M. Yu and T. Shu, "Fault diagnosis method for gearbox based on α-stable distribution parameters and support vector machines," *Measurement and Control Technology*, vol. 31, no. 8, pp. 21–30, 2012.

[29] G. Yu, C. N. Li, and J. F. Zhang, "A new statistical modeling and detection method for rolling element bearing faults based on alpha-stable distribution," *Mechanical Systems and Signal Processing*, vol. 41, no. 1-2, pp. 155–175, 2013.

[30] J. B. Long, H. B. Wang, P. Li, and H. S. Fan, "Applications of fractional lower order time-frequency representation to machine bearing fault diagnosis," *IEEE/CAA Journal of Automatica Sinica*, vol. 99, pp. 1–17, 2016.

[31] J. B. Long, H. B. Wang, and D. F. Zha, "Evoked potential blind extraction based on fractional lower order spatial time-frequency matrix," *Journal of Biomedical Engineering*, vol. 32, no. 2, pp. 269–274, 2015.

[32] Z. J. Lin, D. F. Zha, and J. Sheng, "Blind estimation of evoked potentials based on covariations in non-gaussian noise," *Journal of Biomedical Engineering*, vol. 27, no. 4, pp. 727–730, 2010.

[33] CWRU bearing data center: http://csegroups.case.edu/bearing-datacenter/pages/download-data-file.